

# A study of the correlation between the amplification of the Fe K $\alpha$ line and the X-ray continuum of quasars due to microlensing

L. Č. Popović<sup>1,2</sup>, P. Jovanović<sup>1,2</sup>, E. Mediavilla<sup>3</sup>, A.F. Zakharov<sup>4,5,6</sup>, C. Abajas<sup>3</sup>, J. A. Muñoz<sup>3,7</sup>, G. Chartas<sup>8</sup>

## ABSTRACT

The observed enhancement of the Fe K $\alpha$  line in three gravitationally lensed QSOs (MG J0414+0534, QSO 2237+0305, H1413+117) is interpreted in terms of microlensing, even when equivalent X-ray continuum amplification is not observed. In order to interpret these observations, first we studied the effects of microlensing on quasars spectra, produced by straight fold caustic crossing over standard relativistic accretion disk. The disk emission was analyzed using the ray tracing method, considering Schwarzschild and Kerr metrics. When the emission is separated in two regions (an inner disk corresponding to the Fe K $\alpha$  line and an outer annulus corresponding to the continuum, or vice-versa) we find microlensing events which enhance the Fe K $\alpha$  line without noticeable amplification of the X-ray continuum, but only during a limited time interval. Continuum amplification is expected if a complete microlensing event is monitored. Second, we studied a more realistic case of amplification by caustic magnification pattern. In this case we could satisfactorily explain the observations if the Fe K $\alpha$  line is emitted from the innermost part of the accretion disk, while the continuum is emitted from a larger region. Also, we studied the chromatic effects of microlensing, finding that the radial distribution of temperature in the accretion disk, combined with microlensing itself, can induce wavelength dependent variability of  $\sim 30\%$  for microlenses with very small masses. All these results show that X-ray monitoring of gravitational lenses is a well suited method for studying of the innermost structure of AGN accretion disks.

*Subject headings:* galaxies – microlensing – line profiles – accretion disks

---

<sup>1</sup>Astronomical Observatory, Volgina 7, 11160 Belgrade 74, Serbia

<sup>2</sup>Isaac Newton Institute of Chile, Yugoslavia Branch and Universidad Diego Portales, Chile

<sup>3</sup>Instituto de Astrofísica de Canarias, 382005 La Laguna, Tenerife, Spain

<sup>4</sup>Institute of Theoretical and Experimental Physics, 25, B.Cheremushkinskaya st., Moscow, 117259, Russia

<sup>5</sup>Astro Space Centre of Lebedev Physics Institute, Moscow, Russia

<sup>6</sup>Isaac Newton Institute of Chile, Moscow Branch

<sup>7</sup>Departamento de Astronomía y Astrofísica, Universidad de Valencia, E-46100 Burjassot, Valencia, Spain

<sup>8</sup>Astronomy and Astrophysics Department, Pennsylvania State University, University Park, PA 16802, USA

## 1. Introduction

Recent observational and theoretical studies suggest that gravitational microlensing can induce variability in the X-ray emission of lensed QSOs. Microlensing of the Fe K $\alpha$  line has been reported at least in three macrolensed QSOs: MG J0414+0534 (Chartas et al. 2002), QSO 2237+0305 (Dai et al. 2003), and H1413+117 (Oshima et al. 2001a; Popović et al. 2003a; Chartas et al. 2004).

The influence of microlensing in the X-ray emission has been also theoretically investigated. Mineshige et al. (2001) simulated the variation of the X-ray continuum due to microlensing showing that the flux magnifications for the X-ray and optical continuum emission regions are not significantly different during the microlensing event, while Yonehara et al. (1998, 1999); Takahashi et al. (2001) found that simulated spectral variations caused by microlensing show different behaviour, depending on photon energy. Also, microlensed light curves for thin accretion disks around Schwarzschild and Kerr black holes were considered in Jaroszyński et al. (1992) and microlensing light curves for the Fe K $\alpha$  were simulated by Jaroszyński (2002). On the other hand, the influence of microlensing in the Fe K $\alpha$  spectral line shape was discussed in Popović et al. (2001a); Chartas et al. (2002) and Popović et al. (2003a,b)<sup>1</sup>. Popović et al. (2003a,b) showed that objects in a foreground galaxy with even relatively small masses can produce observable changes in the Fe K $\alpha$  line flux, much stronger than those expected for the UV and optical lines (Popović et al. (2001b); Abajas et al. (2002); Lewis & Ibata (2004)). In the optical spectra, microlensing induced magnification of broad UV lines (e.g., CIV and SIV/OIV) was reported by Richards et al. (2004). Consequently, one can expect that microlensing of the Fe K $\alpha$  line region can be more frequent. Observations of the X-ray continuum and the Fe K $\alpha$  line in multi-imaged AGNs open new possibilities for the study of the unresolved X-ray emitting structure in QSOs, particularly for high redshifted QSOs (Zakharov et al. 2004; Dai et al. 2004).

However, an explanation for different behavior of line and continuum variability in the observed events should be given in context of the microlensing hypothesis. Chartas et al. (2002) detected an increase of the Fe K $\alpha$  equivalent width in the image B of the lensed QSO J0414+0534 that was not followed by the continuum. Chartas et al. (2002) explained the non-enhancement of the continuum emission in the spectrum of image B by proposing that the thermal emission region of the disk and the Compton up-scattered emission region of the

---

<sup>1</sup>Simulations of X-ray line profiles are presented in a number of papers, see, for example, Fabian (2001); Zakharov & Repin (2002a,b,c) and references therein, in particular Zakharov et al. (2003) showed that information about the magnetic field may be extracted from X-ray line-shape analysis; Zakharov & Repin (2003a,b) discussed signatures of X-ray line-shapes for highly inclined accretion disks.

hard X-ray source lie within smaller radii than the iron-line reprocessing region. Analyzing the X-ray variability of QSO 2237+0305A, Dai et al. (2003) also measured amplification of the Fe K $\alpha$  line in component A of QSO 2237+0305 but not in the continuum. However, in this case the interpretation was different. Dai et al. (2003) suggested that the larger size of the continuum emission region ( $\sim 10^{14}$  cm  $\sim 100 R_g$  for  $M_{BH} = 10^7 M_\odot$ ) with respect to the Fe K $\alpha$  emission region ( $\sim 10 R_g$ ) could explain this result. Finally, in H 1413+117 Chartas et al. (2004) found that the continuum and the Fe K $\alpha$  line were enhanced by a different factor.

With the aim of discussing these results, we will model here the behavior of the X-ray continuum and the Fe K $\alpha$  line during a microlensing event for different sizes of the continuum and the Fe K $\alpha$  line emission regions.

## 2. Microlensing of a compact accretion disk

### 2.1. The model

The assumption of a disk geometry for the distribution of the Fe K $\alpha$  emitters is supported by the spectral shape of this line in AGN (e.g. Nandra et al. (1997), where they have investigated the iron line properties of 18 Sy 1 galaxies). Regarding the X-ray continuum emission, it seems that it mainly arises from an accretion disk. For instance, Fabian & Vaughan (2003) have shown that the X-ray spectral variability of MCG-6-30-15 can be modeled by a two-component model where the one varying component is a power-law and the other constant component is produced by very strong reflection from a relativistic disk.

To study the effects of microlensing on a compact accretion disk we will use the ray tracing method considering only those photon trajectories that reach the sky plane at a given observer's angle  $\theta_{\text{obs}}$  (see e.g. Popović et al. (2003a) and references therein). The amplified brightness with amplification  $A(X, Y)$  for the continuum is given by

$$I_C(X, Y; E_{\text{obs}}) = I_P(E_{\text{obs}}, T(X, Y)) \cdot A(X, Y), \quad (1)$$

and for the Fe K $\alpha$  line by

$$I_L(X, Y; E_{\text{obs}}) = \frac{I_P(E_0 \cdot g(X, Y), T(X, Y)) \cdot}{\delta(E_{\text{obs}} - E_0 \cdot g(X, Y)) \cdot A(X, Y)}, \quad (2)$$

where  $T(X, Y)$  is the temperature,  $X$  and  $Y$  are the impact parameters which describe the apparent position of each point of the accretion disk image on the celestial sphere as seen

by an observer at infinity;  $E_0$  is the the line transition energy ( $E_0^{\text{Fe K}\alpha} = 6.4$  keV) and  $g(X, Y) = E_{\text{obs}}/E_{\text{em}}$  is the energy shift due to relativistic effects ( $E_{\text{obs}}$  is the observed energy and  $E_{\text{em}}$  is the emitted energy from the disk). Here we will not consider the cosmological redshift. The emissivity of the disk is one of the important parameters which has influence on the continuum and line shapes. The observed continuum flux is very often fitted with one or two black-body components in the soft X-ray, in addition to the hard X-ray power law (see e.g. Page et al. 2004). The line shape, as well as the continuum distribution, strongly depend on emissivity law. In the standard Shakura-Sunyaev disc model (Shakura & Sunyaev 1973), accretion occurs via an optically thick and geometrically thin disc. The effective optical depth in the disc is very high and photons are close to thermal equilibrium with electrons. The surface temperature is a function of disk parameters and results in the multicolor black body spectrum. This component is thought to explain the 'blue bump' in AGN and the soft X-ray emission in galactic black holes. Although the standard model does not predict the power-law X-ray emission observed in all sub-Eddington accreting black holes, the power law for the X-ray emissivity in AGN is usually accepted (see e.g. Nandra et al. 1999). But one can not exclude other emissivity laws, such as black-body or modified black-body emissivity laws. Therefore, we will use here black-body, modified black-body and power emissivity laws for both; the Fe K $\alpha$  and continuum emission.

In the case of the black-body radiation law, the disk emissivity is given as (e.g. Jaroszyński et al. 1992):

$$I_P(X, Y; E) = B[E, T_s(X, Y)],$$

where

$$B(E, T_s(X, Y)) = \frac{2E^3}{h^2 c^2} \frac{1}{e^{E/kT_s(X, Y)} - 1}, \quad (3)$$

where  $c$  is the speed of light,  $h$  is the Planck constant,  $k$  is the Boltzmann constant and  $T_s(X, Y)$  is the surface temperature of X-ray accretion disk.

In principle, one can assume different distribution of the surface temperature along disk. To obtained the X-ray continuum distribution using Eq. (3) one can assume that  $T_s = \text{const.}$ , taking that the black hole is powerful X-ray sources with an effective temperature  $10^7$  to  $10^8$  K. But, regarding the standard disk model it is expected that the surface temperature at least is radially dependent. Therefore, here we will accept the radial distribution of surface temperature given by (Shakura & Sunyaev 1973):

$$T_s(X, Y) \sim r^{-3/2}(X, Y)(1 - r^{-1/2}(X, Y))^{4/5} \text{ K}, \quad (4)$$

taking that an effective temperature is in an interval from  $10^7$  to  $10^8$  K. The distribution of the temperature along the radius of the disk used in this paper is given in Fig. 1 (top) and

corresponding shape of spectral energy distribution is shown in Fig. 1 (bottom). In Eq. (4)  $r$  is the dimensionless parameter defined as:

$$r(X, Y) = \frac{R(X, Y)}{6R_g} = \frac{1}{6} \frac{R(X, Y)c^2}{GM} = \frac{M_\odot}{M} \frac{R(X, Y)}{9 \text{ km}},$$

where  $R(X, Y)$  is disk radius, expressed in gravitational radii  $R_g$ .

However, in the innermost part of the accretion disk the Planck function cannot be used properly. Therefore we will use also the standard (classical) Shakura – Sunyaev approach, where the emissivity law is described by a "modified" black-body radiation law (Eqs. (3.4), (3.8) in Shakura & Sunyaev (1973); see also the discussion in Novikov & Thorne (1973); Shapiro & Teukolsky (1983); Straumann (1984))

$$I_P(E; X, Y) \propto x^3 \exp(-x), \quad (5)$$

where  $x = E/kT(X, Y)$ . Shalyapin et al. (2002) used similar expressions to study microlensing in the optical continuum. Taking into account that the observed hard X-ray continuum has a power-law type spectral shape, we will also assume that the time-independent intrinsic emissivity of the continuum is:

$$I(E, r) \sim E^{-\Gamma} \times r^{-\alpha},$$

where, according to the investigation of observed X-ray spectra,  $\Gamma$  and  $\alpha$  are taken to be 1.5 and 2.5 (see e.g. Dovčiak et al. 2004). For the Fe K $\alpha$  emission in this case we used the same calculation as in Popović et al. (2003a,b).

We should note here, that disk may be considered to be composed of a number of distinct parts with different physical conditions (e.g. radiation pressure dominant part, matter pressure dominant part, etc. see e.g. Shakura & Sunyaev 1973). Consequently, in general one can expect that the disk can be described by different emissivity laws in different parts (e.g. the black-body law may be applied in outer part of the disk). Taking into account a huge number of parameters which should be considered in the case of microlensed disk (see the next section), we will consider only one emissivity law for whole disk.

The total observed flux for the continuum and the Fe K $\alpha$  line is given as

$$F(E) = \int_{\text{image}} [I_C(X, Y; E) + I_L(X, Y; E)] d\Omega, \quad (6)$$

where  $d\Omega$  is the solid angle subtended by the disk in the observer's sky and the integral extends over the whole emitting region.

As one can see from Eq. (7) the total observed flux is a sum of the continuum and the line fluxes, consequently, the amplification in the continuum and in the Fe K $\alpha$  line can be considered separately as two independent components. On the other hand, the amplifications will depend on the sizes and geometry of the continuum and line emitting regions. In further text we will consider amplifications in the line and in the continuum separately.

We would like to point out here that the aim of the paper is not to create the perfect accretion disk model (taking into account different effects that can be present as e.g. opacity of the disk, spots in the disk etc.), but only to illustrate the influence of microlensing on the continuum and the Fe K $\alpha$  line amplification and demonstrate that this phenomenon could essentially change general conclusions. Therefore, we will use the three emissivity laws of the disk and the very important effect of strong gravitation (beaming and light-bending in Schwarzschild and Kerr metrics).

## 2.2. Disk and microlens parameters

To apply the model one needs to define a number of parameters that describe the emission region and the deflector. In principle, we should find constraints for the: size of the disk emission region, disk inclination angle, mass of the black hole, accretion rate, relative amplification, the constant  $\beta$  (Chartas et al. 2002, Popović et al. 2003), orientation of the caustic with respect to the rotation axis, direction of the caustic crossing and microlens mass. In the following subsections we choose and discuss the parameters used in the calculations.

### 2.2.1. Accretion disk parameters

For the disk inclination we adopt the averaged values given by Nandra et al. (1997) from the study of the Fe K $\alpha$  line profiles of 18 Seyfert 1 galaxies:  $i = 35^\circ$ . The inner radius,  $R_{in}$ , can not be smaller than the radius of the marginally stable orbit,  $R_{ms}$ , that corresponds to  $R_{ms} = 6R_g$  (gravitational radii,  $R_g = GM/c^2$ , where  $G$  is gravitational constant,  $M$  is the mass of central black hole, and  $c$  is the velocity of light) in the Schwarzschild metric and to  $R_{ms} = 1.23R_g$  in the case of the Kerr metric with angular momentum parameter  $a = 0.998$ . To select the outer radius,  $R_{out}$ , we take into account previous investigations of the X-ray variability that support very compact X-ray emitting disks. In particular, Oshima et al. (2001b) from the observed variation in the lensed blazar PKS 1830-211 infer a size of the X-ray continuum emission region of  $\sim 3 \times 10^{14}$  cm, that is in agreement with estimation for QSO 2237+03050 given by Dai et al. (2003). So, considering a range of black hole masses

of  $10^7 - 10^9 M_{\odot}$  we can conclude that the X-ray emission is coming from a compact region of the order of 10 to 100  $R_g$ . This range of sizes is also acceptable for the Fe K $\alpha$  emission region (see e.g. Nandra et al. (1997, 1999)).

To explore the suitability of the various hypothesis explaining the lack of adequate response of the X-ray continuum to the microlensing events detected in the Fe K $\alpha$  line (see §1), we are going to consider several combinations of disk sizes for the emitters of both the continuum and the line: (i) the inner and outer radii of both emission regions are the same,  $R_{in} = R_{ms}$  and  $R_{out} = 20 R_g$ ; (ii) the inner radius is the same,  $R_{in} = R_{ms}$ , but the outer radius of the X-ray continuum disk is smaller,  $R_{out} = 20 R_g$ , than the radius of the line emission disk,  $R_{out} = 80 R_g$ ; (iii) the continuum emission disk has radii  $R_{in} = R_{ms}$ ,  $R_{out} = 20 R_g$  and the line emission disk  $R_{in} = 20 R_g$  and  $R_{out} = 80 R_g$  (the continuum emission takes place in an inner part of disk surrounded by an annulus of Fe K $\alpha$  emission); (iv) the continuum emission disk has radii  $R_{in} = 20 R_g$ ,  $R_{out} = 80 R_g$  and the line emission disk  $R_{in} = R_{ms}$  and  $R_{out} = 20 R_g$  (the Fe K $\alpha$  emission is located in the inner disk and the continuum emission in the outer annulus).

We adopt the central object mass and accretion rate from Bian & Zhao (2002). We assume a black hole of mass  $M_8 = 10^8 M_{\odot}$  and accretion rate  $\dot{m} = 0.4$  in Eddington units ( $\dot{m} = \frac{1.578 \dot{M}_{26}}{3.88 M_8}$ ). We will use this value in order to determine the effective temperature distribution. These values are in agreement with Wang et al. (2003) where it was found that the majority of QSOs have black hole masses in the range of  $10^8 - 10^9 M_{\odot}$ , and accretion rates ranging from 0.01 to 1 in units of the Eddington accretion rate.

It is difficult to discuss the validity of different emissivity laws for demonstration of the X-ray emission (in the line as well as in the continuum), but sometimes, as for example in the case of black-body emissivity law, the emissivity at X-ray wavelengths can be extremely small compared with, for example, optical wavelengths, and X-ray photons are emitted from a quite small region. In Fig. 1 (bottom), we presented the continuum shapes for different emissivity laws used in the calculation (maximum of each is normalized to one). The shapes of the continuum were calculated for different dimensions of the disk. As one can see from Fig. 1 (bottom), the shape of the continuum strongly depends not only on emissivity law, but also on disk dimensions.

### 2.2.2. *Microlens model and parameters*

Different types of caustics can be used to explain the observed microlensing events in quasars. Moreover, for the exact event one can model the caustic shape to obtain different

parameters (see e.g. Abajas et al. 2004, Kochanek 2004 for the case of Q2237+0305). In order to apply an appropriate microlens model, first we will consider a standard microlensing magnification pattern (Figure 2, left) for the Q2237+0305A image with 16 Einstein ring radii (ERR) on a side and  $\kappa = 0.36$ ,  $\lambda = 0.40$  and  $\kappa_c = 0$ . The mass of microlens is taken to be  $1M_\odot$ . The simulation was made employing ray-shooting techniques that send rays from the observer through the lens to the source plane (Kayser et al. 1986; Schneider & Weiss 1987; Wambsganss et al 1990a,b). We assume a flat cosmological model with  $\Omega = 0.3$  and  $H_o = 70 \text{ km s}^{-1}\text{Mpc}^{-1}$ .

In Figure 2 we presented a comparison between the projected magnification map in the source plane and an accretion disk with a size of  $1000 R_g$  (presented as a circle in Figure 2, right). Taking into account the small dimensions of the X-ray emission region (several  $10s R_g$ ) the approximation of a straight fold caustic can be assumed for this pattern. We explored the general behavior of the total continuum and Fe K $\alpha$  flux amplification due to microlensing. First we used the straight fold caustic approximation. (see Eqs. (5)-(8) in Popović et al. (2003a)). We also considered an example assuming a caustic magnification pattern for the Q2237+0305A image produced by a population of low mass microlens in §3.3.

In Table 1 we give the projected Einstein Ring Radii (ERR) for the lensed QSOs where amplification of the Fe K $\alpha$  line (MG J0414+0534, Chartas et al. (2002); QSO H1413+117, Oshima et al. (2001a); Chartas et al. (2004) and QSO 2237+0305, Dai et al. (2003)) has been observed. The ERRs (expressed in gravitational radii) are computed for different deflector masses and for a black hole mass of  $10^8 M_\odot$ . We found that even deflectors with small mass have ERR with sizes from several tens to several hundreds of gravitational radii. To obtain a qualitative understanding of the influence of the microlens mass on our results we consider microlens masses that correspond to ERR values equal to  $50 R_g$  (see Figs. 3-7). Qualitatively the shape of the flux amplification will not be changed if we consider massive deflectors (e.g.  $\text{ERR}=2000 R_g$ , see Fig. 8). Even if we apply simple assumption of the straight-fold caustic, we should define the caustic parameters  $A_0$  and  $\beta$ . These values can be considered to be different for different microlensing events. Higher values of  $A_0$  and  $\beta$  will cause higher amplification. Here we would like to demonstrate correlation between the line and flux amplification due to microlensing and we will adopt values considered in more details by Chartas et al. (2002)  $A_0=1$  and  $\beta=1$  (Witt et al. 1993). Here we considered three directions of caustic crossing; parallel ( $Y=0$ ) and perpendicular ( $X=0$ ) to the rotation axis as well as in a direction inclined  $45^\circ$  with respect to the rotation axis ( $X=Y$ ).

### 3. Results and Discussion

#### 3.1. Continuum and line profile variability

In Figures 3 and 4 we present the variations of the total X-ray emission spectra (continuum + Fe K $\alpha$  line) during a straight fold caustic crossing ( $A_0=1$ ,  $\beta=1$  and  $\text{ERR}=50 R_g$ ). The radial dependence of the emissivity is related to the black body radiation law (see §2). In Figure 3 the sizes of the continuum and line emission regions are the same,  $R_{\text{inn}} = R_{\text{ms}}$  and  $R_{\text{out}} = 20 R_g$ . In Figure 4, the Fe K $\alpha$  line emitting disk is larger:  $R_{\text{out}} = 80 R_g$ . We consider both metrics, Schwarzschild and Kerr. We simulate the caustic crossing perpendicular to (first and second rows) and along (third and fourth rows) the rotation axis in both directions;  $\kappa = \pm 1$ , respectively.

#### 3.2. Integrated flux variability

In Figures 5-8 we present the variation of the integrated flux (normalized to the integrated flux in the absence of microlensing) for both, the X-ray continuum and the Fe K $\alpha$  line during straight fold caustic crossings (considering that the amplification outside the caustic  $A_0=1$ , as well as  $\beta=1$  and  $\text{ERR}=50 R_g$ , see Figure captions). We considered all three emissivity laws (see §2.1) Figures 5a,b correspond to case (ii) of §2.2.1, Figures 5c,d and 7 (left) to case (iii) and Figures 6 and 7 (right) to case (iv). (Case (i) is the same for line and continuum; it corresponds to the continuum variation in Figures 5a,b). In Fig. 7, we present cases (iii) and (iv) where a power-law emission is taken into account. In Figure 8 a very favorable case of high ERR and inclination is considered for case (iii) of §2.2.1. Notice that FeK $\alpha$  microlensing events were observed in BAL QSOs which may have highly inclined accretion disks;  $i \approx 75^\circ$ .

As one can see from Figure 8 (as it also was shown in Popović et al. 2003a,b) the amplified component is mainly very narrow in comparison with the undeformed line. This result is in agreement with the observations of Chartas et al. (2002, 2004) and Dai (2003) and supports the conclusions of these authors that enhancement of the Fe K $\alpha$  line observed in only one of the images of a lensed quasar was caused by microlensing.

Some interesting results can be inferred from our exploratory work: (a) when both the line and continuum disk profiles have the same inner radius, the differences in outer radius cannot cause significant differences in the total line and the continuum flux variation (see Figs. 5a,b) for the considered emission laws, (b) when we separate the emission considering an inner disk contributing to the continuum and an outer annulus contributing to the Fe

$K\alpha$  line (or vice-versa) we found significant differences between the continuum and the line amplification (see Figures. 5c,d, 6 – 8), (c) the results are qualitatively similar for all considered emissivity laws (see Figs. 5-8), (d) interchanging between Schwarzschild and Kerr metrics induces only slight differences in normalized flux amplification (see Figs. 5-7).

Figures 5-8 were intended to explore the two scenarios suggested by Dai et al. (2003) and Chartas et al. (2002) to explain the non observed associated enhancement of the X-ray continuum in objects with a microlensed Fe  $K\alpha$  line. This behavior can be expected in case (iii) when the microlens crosses the outer part of the disk (Figures 5c,d and the right panel of Fig. 7) and in case (iv) when the microlens crosses the inner part of the disk (see Fig. 6 and the left panel of Fig. 7). However, in none of the Figures does the continuum remain strictly constant during a complete Fe  $K\alpha$  microlensing event. In the most favorable case (the inner Fe  $K\alpha$  disk plus an outer continuum annulus; Fig. 6 and 7) we achieve a significant and relatively quick change of the Fe  $K\alpha$  emission while the continuum experiences only a slow increase. This behavior could well approximate a non-varying continuum but only if we consider observations in a temporal window that fall on the peak of the microlensing event in the Fe  $K\alpha$  line. In this case the continuum of the microlensed image experiences an (slowly changing or almost constant) amplification with respect to the continua of the other images, but practically it is indistinguishable from the amplifications due to global macrolensing.

### 3.3. Microlensing by a caustic magnification pattern: An example for Q2237+0305A image

Here we consider a situation where a low mass population of microlenses (smaller than one solar mass) can form pattern structures (see Table 1) which are comparable with the size of the X-ray accretion disk. Moreover, the black hole mass of the lensed quasar may be of the order of  $10^{9-10} M_\odot$ , taking that  $R_g \sim M_{BH}$ , the pattern structure of low mass microlenses are comparable with a X-ray disk size of several dozens  $R_g$ . Therefore, here we consider that the black hole mass of the lensed quasar is  $10^9 M_\odot$ .

For modeling of the caustic magnification pattern for image Q2237+0305A we used the same values for the convergence and external shear as presented in Figure 2, but for a low mass population, taking that the mass of the deflectors are randomly distributed in an interval ranging from  $0.1 M_\odot$  to  $0.6 M_\odot$ , with a mean value of  $\langle m \rangle = 0.35 M_\odot$ . Also, the positions of the lenses were distributed randomly in a rectangular region in the lens plane, significantly larger than the considered region in the source plane. Now, 1 $ERR$  projected in the source plane corresponds to

$$ERR(M) = ERR(M_{\odot}) \sqrt{\frac{M}{M_{\odot}} \frac{M_8}{M_{BH}}},$$

where  $ERR(M_{\odot}) = 0.054\text{pc}$  is the projected ERR for a solar mass deflector,  $M$  is the mean mass of the deflectors and  $M_{BH}$  is the black-hole mass. Taking the mean deflector mass as  $\langle m \rangle = 0.35 M_{\odot}$  and  $R_g = 9.547 \cdot 10^{-6} M_{BH}/M_8$  pc, we modeled a caustic magnification pattern of  $1\text{ERR} \times 2\text{ERR}$ , that corresponds to  $334.63R_g \times 669.26R_g$  in the source plane for a black hole mass of  $M_{BH} = 10^9 M_{\odot}$  (Fig. 9). For numerical reasons, the microlens magnification map is given in pixels,  $1000 \times 2000$  (1pix =  $0.33463R_g$  in source plane). As one can see from Figure 9, the microlensing pattern structures are comparable with a compact X-ray accretion disk.

In our previous modeling based on the straight fold caustic approximation the lack of a correlation between the continuum and Fe K $\alpha$  line is expected only if the line and X-ray continuum region are separated. Recent investigations of the Fe K $\alpha$  line profile from active galaxies show that the line should be emitted from the innermost part of the accretion disk. In particular, Ballantyne & Fabian (2005) found that in BLRG 4C+74.26 the outer radius of the relativistic iron line should be within  $10 R_g$ . Consequently, here we will assume that the Fe K $\alpha$  line is formed in the innermost part of the disk ( $R_{\text{inn}} = R_{\text{ms}}$ ;  $R_{\text{out}} = 20 R_g$ ) and that the continuum (emitted in the energy range between 0.1 keV and 10 keV) is mainly originated from a larger region ( $R_{\text{inn}} = 20 R_g$ ;  $R_{\text{out}} = 100 R_g$ ).<sup>2</sup> On the other hand, from the straight fold caustic modeling we conclude that the correlation between the total line and continuum flux due to microlensing is not very different for different emissivity laws. Consequently, here we used the black-body emissivity law. A disk (Schwarzschild metric) with an inclination of  $35^{\circ}$  is considered.

To explore the line and X-ray continuum variation we moved the disk center along the microlensing map as it is shown in Figure 9 (from left to the right corresponding 0 to 2000 pixels). In Figure 10 we present the corresponding total line and X-ray continuum flux variation. As one can see from Figure 10, there is a global correlation between the total line and continuum flux during the complete path. However, the total continuum flux variation is smooth and has a monotonic change, while the total line flux varies very strongly and randomly.

In fact, during some portion of the microlensing of the emission regions by the magnifi-

---

<sup>2</sup>Note here, taking the continuum disk size from  $R_{\text{inn}} = 20 R_g$  to  $R_{\text{out}} = 100 R_g$ , we neglected the contribution of the innermost part emission (from  $R_{\text{ms}}$  to  $20 R_g$ ) to the total continuum flux only in the energy interval from 0.1 keV to 10 keV. It does not mean that there is no the continuum emission.

cation pattern, we found the total Fe K $\alpha$  line flux changes, while the continuum flux remains nearly constant (e.g. the position of the disk center between 1000 and 1200 pixels). This and the shapes of the line and continuum total flux amplification indicate that the observed microlensing amplification of the Fe K $\alpha$  in three lensed quasars may be explained if the line is originated in the innermost part of the disk and the X-ray continuum in a larger region. Also, it seems that the contribution of the continuum emitted from the innermost part of the disk (within  $10 R_g$ ) to the total continuum (in the energy interval from 0.1 to 10 keV) flux is not significant. Further observations are needed to provide more data which might be compared with our theoretical results.

### 3.4. Wavelength dependence of the X-ray continuum amplification

The influence of gravitational microlensing on the spectra of lensed QSOs was discussed in several papers (see Popović and Chartas 2005, and references therein). Mainly, the color index was calculated as an indicator of the microlensing (see e.g. Wambsganss & Paczynski 1991, Wyithe et al. 2000) as well as amplified flux behaviors (see Yonehara et al. 1998, Yonehara et al. 1999, Takahashi et al. 2001) of a disk, but the exact shape of the amplification as a function of wavelength (or energy) for a partly microlensed disk has not been calculated. Here, taking into account that the emitters at different radii in the accretion disk have different temperatures (see Fig. 1) and make different contributions to the observed continuum flux at a given wavelength, we calculated the amplification as a function of observed energies. During a caustic crossing microlensing effects would depend on the location of the emitters and, consequently, would induce a wavelength dependence in the amplification. This dependence can be clearly appreciated in the spectra of Figures 3, 4 and 8. In Figures 11ab-12ab we present the amplification as a function of the observed energies for an accretion disk with the characteristics given in §2.2.1, with inner radius  $R_{in} = R_{ms}$  and outer radius  $R_{out} = 30 R_g$ , assuming caustic crossing along the rotation axis (X). We have considered the black body (Fig. 11ab) and the modified black body (Fig. 12ab) emissivity laws for both Schwarzschild and Kerr metrics.

As it can be seen in Figures 11-12 the amplification is different for different observed energies. The amplification is higher for the hard X-ray continuum when the caustic crosses the central part of the disk (see Fig. 12). Depending mainly on the caustic location and on the emissivity law selected the difference of the amplification in the energy range studied by us can be significant (e.g.  $\sim 20\%$  for very small mass microlenses,  $ERR=50R_g$ , see Figs. 11-12). This effect could induce a noticeable wavelength dependent variability of the X-ray continuum spectrum during a microlensing event (of even a 30%), providing a tool to study

the innermost regions of accretion disks.

#### 4. Conclusions

We have developed a model of microlensing by a straight fold caustic of a standard accretion disk in order to discuss the observed enhancement of the Fe K $\alpha$  line in the absence of corresponding continuum amplification found in three lensed QSOs. Here we summarize several interesting results inferred from our straight fold caustic simulations.

1 - As expected both the Fe K $\alpha$  and the continuum may experience significant amplification by a microlensing event (even for microlenses of very small mass). Thus, the absence of adequate continuum amplification in the observed Fe K $\alpha$  microlensed QSOs should be related to the structure of the accretion disk and/or the geometry of the event.

2 - Extending the outer radius of the distribution of Fe K $\alpha$  emitters does not result in any significant changes in our results. This is due to the radial dependence of the emissivity as expressed in the standard accretion disk model (Shakura & Sunyaev 1973) that concentrates the emission near the center of the black hole making negligible the contribution from the outer parts to the integrated flux. In principle we could consider other less steep emissivity laws that make the outer parts of the disk more important, however previous studies (e.g. Nandra et al. (1999)) support the hypothesis of a strong emissivity gradient.

3 - Segregation of the emitters allows us to reproduce the Fe K $\alpha$  enhancement without equivalent continuum amplification if the continuum emission region lies interior to the Fe K $\alpha$  emission region or vice versa but only during limited time intervals. In fact, in none of the simulations does the continuum remain constant during a complete Fe K $\alpha$  microlensing event. In the case of an inner Fe K $\alpha$  disk plus an outer continuum annulus a significant change of the Fe K $\alpha$  emission is obtained while the continuum experiences only a very shallow gradient. This behavior could well approximate the detected non-varying continuum for observations covering only the peak of the Fe K $\alpha$  microlensing event.

4 - We have also studied a more realistic case of microlensing by a caustic magnification pattern assuming a population of low mass deflectors. In this case we can successfully reproduce the observed lack of correlation between the X-ray continuum and Fe K $\alpha$  emission amplification only if the line and continuum emission regions are separated.

An extreme case of segregation is that of the two component model for the continuum suggested in several papers (see e.g. (Fabian & Vaughan 2003; Page et al. 2004) if the contribution of the disk component to the X-ray continuum were weak enough.

5 - We have studied the chromatic effects of microlensing in the X-ray continuum and find that the dependence with wavelength of the amplification can induce, even for small mass micro-deflectors ( $ERR=50R_g$ ), chromatic variability of about 30% in the observed energy range (from 0.1 keV to 10 keV) during a microlensing event.

Further observations of the lensed quasars in the X-ray are needed to confirm these results. In any case monitoring of gravitational lenses may help us to understand the physics of the innermost part of the relativistic accretion disks.

This work is a part of the projects: P1196 "Astrophysical Spectroscopy of Extragalactic Objects" supported by the Ministry of Science, Technologies and Development of Serbia and P6/88 "Relativistic and Theoretical Astrophysics" supported by the IAC. LČP was supported by Alexander von Humboldt Foundation through the program for foreign scholars. JAM is a *Ramón y Cajal Fellow* from the MCyT of Spain. Also, we would like to thank the anonymous referee for very useful comments.

## REFERENCES

Abajas, C., Mediavilla, E.G., Muñoz, J.A., Popović, L. Č., & Oscoz A. 2002, ApJ 576, 640.

Abajas, C., Mediavilla, E.G., Gil-Merino, R., Muñoz, J.A., Popović, L. Č., & Oscoz A. 2004, presented in IAU 225 Symposium "Impact of Gravitational Lensing on Cosmology", 19-23 July, Lausanne, Switzerland.

Ballantyne D.R., Fabian, A.C. 2005, ApJ, 622, L97.

Bian, W., Zhao, Y. 2002, A&A, 395, 465.

Chartas, G., Agol, E., Eracleous, M., Garmire, G., Bautz, M. W., Morgan, N. D. 2002, ApJ, 568, 509.

Chartas, G., Eracleous, M., Agol, E., Gallagher, S. C. 2004, ApJ, 606, 78.

Dai, X., Chartas, G., Agol, E., Bautz, M. W., & Garmire, G.P. 2003, ApJ, 589, 100.

Dai, X., Chartas, G., Eracleous, M. & Garmire, G.P. 2004, ApJ, 605, 45.

Dovčiak, M., Karas, V., Yaqoob, T. 2004, ApJS, 153, 205.

Fabian, A. 2001, in Proc. of the 20th Texas Symposium on Relativistic Astrophysics, ed. J. C. Wheeler, H. Martel, AIP Conferences, 586, (American Institute of Physics, Melville, New York) 643.

Fabian, A.C., Vaughan S. 2003, MNRAS, 340, L28.

Jaroszyński, M. 2002, Acta Astronomica, 52, 203.

Jaroszyński, M., Wambsganss, J.W., Paczyński, B. 1992, ApJ, 396, L65.

Kayser, R., Refsdal, S., & Stabell, R. 1986, A&A, 166, 36.

Kochanek, C.S. 2004, ApJ, 605, 58.

Lewis, G. F., Ibata, R.A. 2004, MNRAS, 348, 24.

Mineshige, S., Yonehara, A., & Takahashi, R. 2001, PASA, 18, 186.

Nandra K., George I.M., Mushotzky R.F., Turner T.J. & Yaqoob T. 1997, ApJ. 477, 602.

Nandra, K., George, I. M., Mushotzky, R. F., Turner, T. J., Yaqoob, T. 1999, ApJ 523, 17.

Novikov, I.D., & Thorne, K.S. 1973, Black Holes (Eds. C. De Witt, B. De Witt), Gordon & Breach, 344.

Oshima, T., Mitsuda, K., Fujimoto R., Iyomoto N., Futamoto K., et al. 2001a, ApJ, 563, L103.

Oshima, T., Mitsuda, K., Ota, N., Yonehara, A., Hattori, M., Mihara, T. & Sekimoto, Y. 2001b, ApJ, 551, 929.

Page, K.L., Reeves, J.N., O'Brien, P.T., Turner, M.J.L., Worrall, D.M. 2004, MNRAS, 353, 133.

Popović, L. Č., Chartas, G. 2005, MNRAS, 357, 135.

Popović, L., Č., Mediavilla, E.G., Muñoz J., Dimitrijević, M.S., & Jovanović, P. 2001a, SerAJ, 164, 73.

Popović, L.Č., Mediavilla, E.G., & Muñoz J. 2001b, A&A 378, 295.

Popović, L.Č., Mediavilla, E.G., Jovanović, P., & Muñoz, J.A. 2003a, A&A, 398, 975.

Popović, L.Č., Jovanović, P., Mediavilla, E.G., & Muñoz, J.A. 2003b, Astron. Astrophys. Transactions, 22, 719.

Richards, G.T., Keeton, C.R., Pindor, B. et al. 2004, ApJ, 610, 679.

Schneider, P., & Weiss, A. 1987, A&A, 171, 49.

Shakura, N.I., & Sunyaev, R.A. 1973, A&A, 24, 337.

Shalyapin, V., N., Goicoechea, L., J., Alcalde, D., Mediavilla E., Muñoz J.A., Gil-Merino, R. 2002, ApJ, 579, 127.

Shapiro, S.L., & Teukolsky, S.A. 1983, Black Holes, White Dwarfs and Neutron Stars: Physics of Compact Objects, John Wiley & Sons, New York.

Straumann, N. 1984, General Relativity and Relativistic Astrophysics, Springer-Verlag, Berlin, Heidelberg, New York.

Takahashi, R., Yonehara, A., Mineshige, S. 2001, Publ. Astron. Soc. Japan 53, 387.

Wang, J.-M., Ho, L. C.; Staubert, R. 2003, A&A, 409, 887.

Wambsganss, J., Paczynski, B. 1991, AJ, 102, 86.

Wambsganss, J., Paczynski, B., & Katz, N. 1990a, ApJ, 352, 407.

Wambsganss, J., Schneider, P., & Paczynski, B. 1990b, ApJ, 358, L33.

Witt H.J., Kayser R., Refsdal S., 1993, A&A 268, 501.

Wyithe, J. S. B., Webster, R. L., Turner, E. L., Agol, E. 2000, MNRAS, 318, 1105.

Yonehara, A., Mineshige, S., Fukue, J., Umemura, M., Turner, E.L. 1999, A&A, 343, 41.

Yonehara, A., Mineshige, S., Manmoto, T., Fukue, J., Umemura, M., Turner, E.L. 1998, ApJ, 501, L41; ApJ, 511, L65.

Zakharov, A.F., Kardashev, N.S., Lukash, V.N., & Repin, S.V. 2003, MNRAS, 342, 1325.

Zakharov, A.F., & Repin, S.V. 2002a, Astronomy Reports, 46, 360.

Zakharov, A.F., & Repin, S.V. 2002b, in Proc. of the Eleven Workshop on General Relativity and Gravitation in Japan, ed. J. Koga, T. Nakamura, K. Maeda, K. Tomita, (Waseda University, Tokyo) 68.

Zakharov, A.F., & Repin, S.V. 2002c, in Proc. of the Workshop "XEUS - studying the evolution of the hot Universe", ed. G. Hasinger, Th. Boller, A.N. Parmar, MPE Report 281, 339.

Zakharov, A.F., & Repin, S.V. 2003a, Nuovo Cim., 118B, 1193.

Zakharov, A.F., & Repin, S.V. 2003b, A&A, 406, 7.

Zakharov, A.F., Popović, L. Č., Jovanović, P. : 2004, A&A, 420, 881.

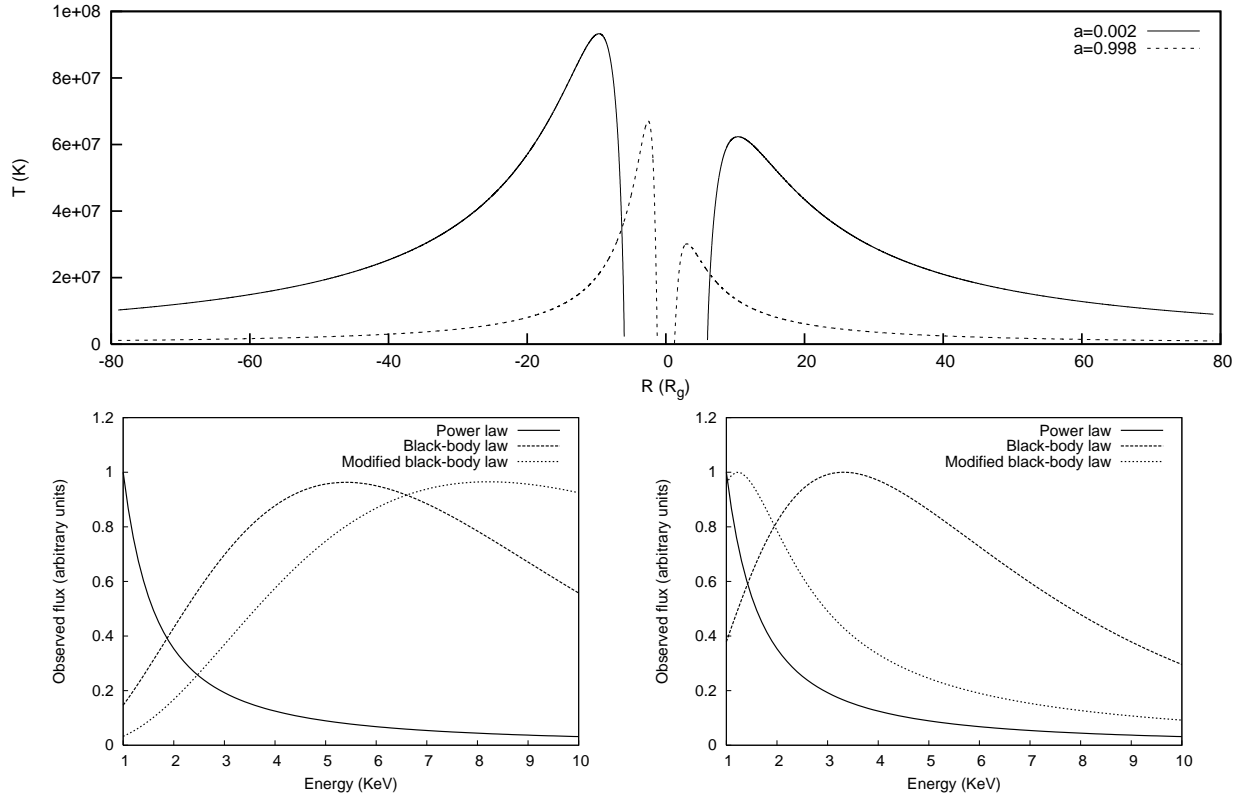


Fig. 1.— Top: The distribution of the temperature as a function of the radius along the direction of the disk rotation, given for two different values of angular momentum  $a$ . Negative values of  $R$  correspond to the approaching and positive values to the receding side of the disk. Bottom: Shapes of the continuum for considered three emissivity laws (normalized to the maximal value) for an accretion disk with outer radius of  $20 R_g$  (left) and  $80 R_g$  (right). The other parameters of the disk are given in §2.2.1.

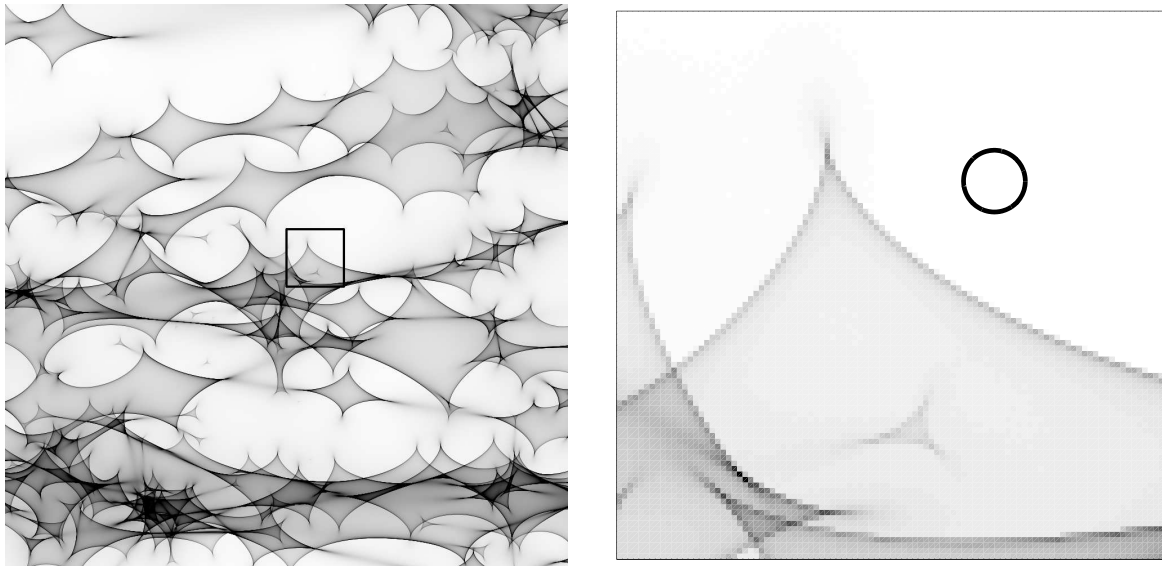


Fig. 2.— *Left*: Microlensing map of QSO 2237+0305A image with 16 ERR (177372  $R_g$ ) on a side (Abajas et al. 2004). *Right*: the small part (square in Figure left) of the microlensing pattern, compared to a face-on accretion disk. The assumed outer radius of the disk is  $R_{out} = 1000 R_g$ .

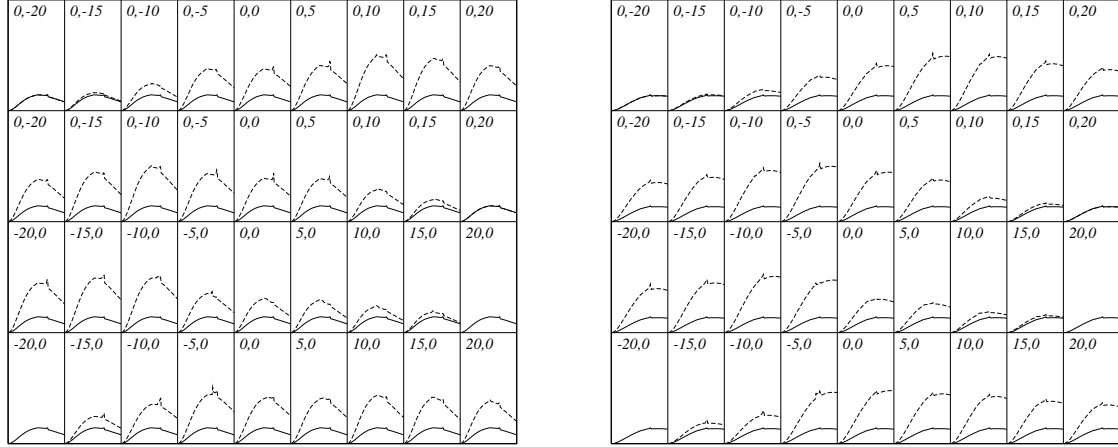


Fig. 3.— Simulations of the behavior of the Fe K $\alpha$  line and continuum variations due to microlensing by a caustic in the case of Schwarzschild (left) and Kerr (right) metrics. The parameters of the caustic are:  $A_0=1$ ,  $\beta=1$  and  $\text{ERR}=50 R_g$ . In the first and second rows we present the caustic crossing perpendicular to the rotating axis for  $\kappa = \pm 1$ , respectively. In the third and fourth rows we show the caustic crossing along the rotation axis with  $\kappa = \pm 1$ , respectively. The radii of the continuum and the Fe K $\alpha$  line emission accretion disks are the same:  $R_{in} = R_{ms}$  and  $R_{out} = 20 R_g$  (where  $R_g = GM/c^2$ ). The unperturbed and normalized emission correspond to solid and dashed lines, respectively. The relative intensity ranges from 0 to 7 (y-axis) and the energy interval from 0.1 to 10 keV (x-axis).

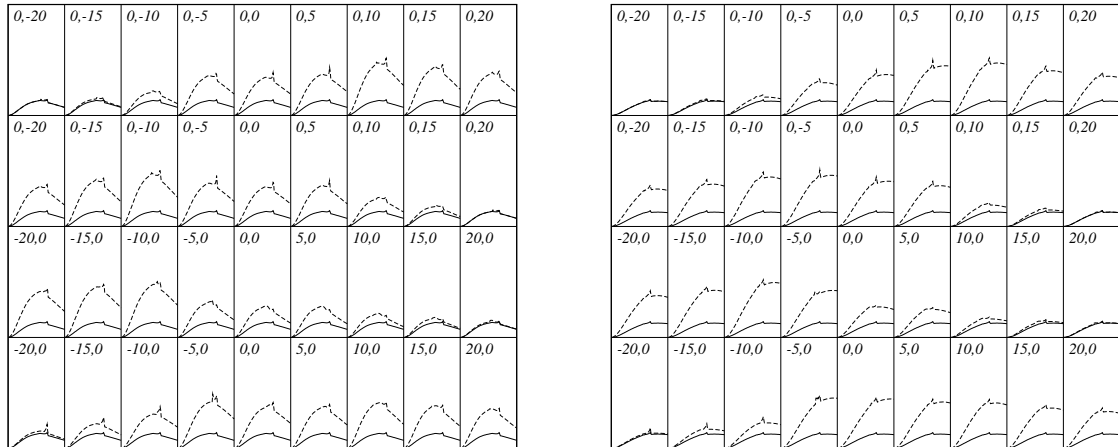


Fig. 4.— As in Fig. 3, but  $R_{out} = 80 R_g$  for the Fe K $\alpha$  line.

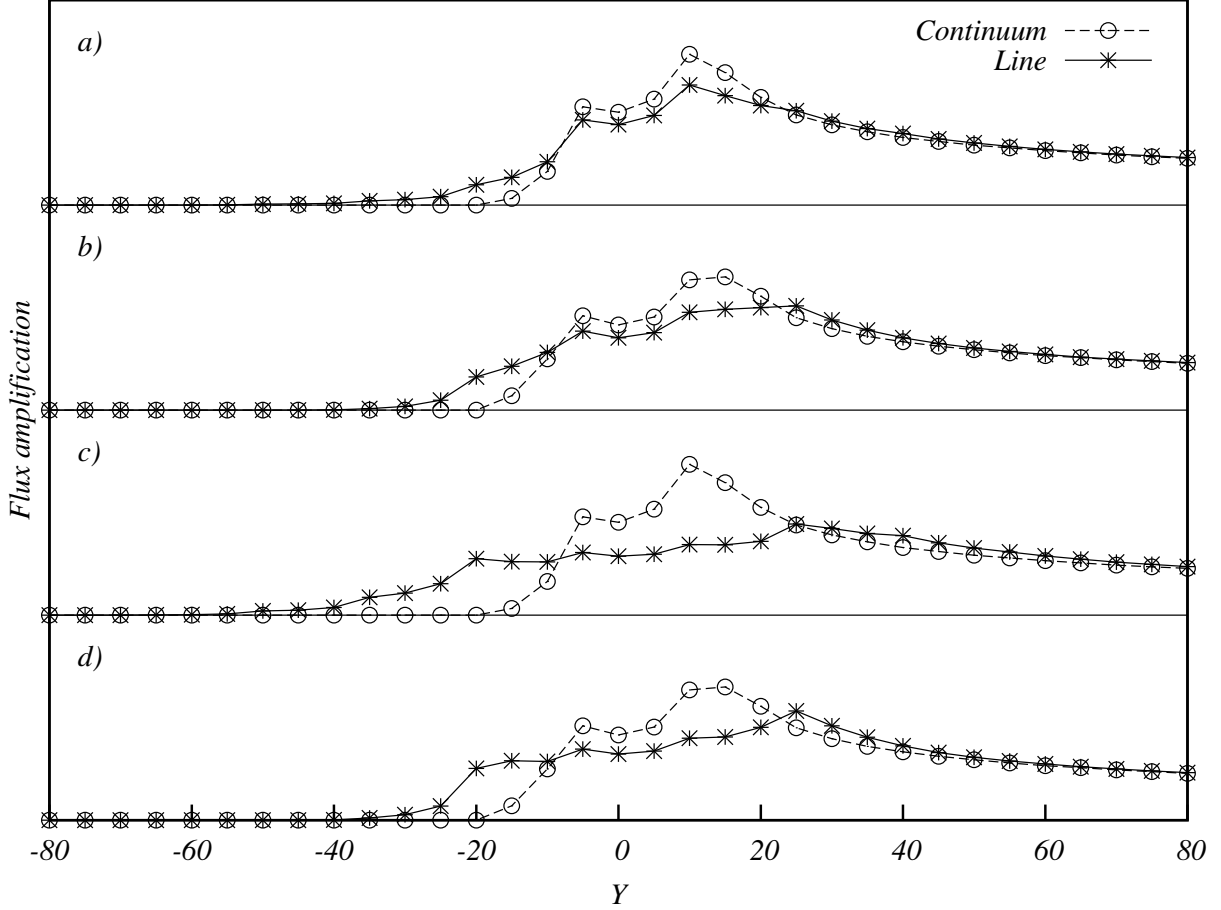


Fig. 5.— Variations of the Fe K $\alpha$  line and X-ray continuum flux due to caustic crossing (ERR=50  $R_g$ ) perpendicular to the rotation axis ( $X=0$ ) for different positions of the caustic in the  $Y$  axis (Schwarzschild metric). Panels correspond to: (a) black body law and case (ii) of §2.2.1, (b) modified black body law and case (ii), (c) black body law and case (iii), (d) modified black body law and case (iii). The flux axis ranges from 1 to 1.7.

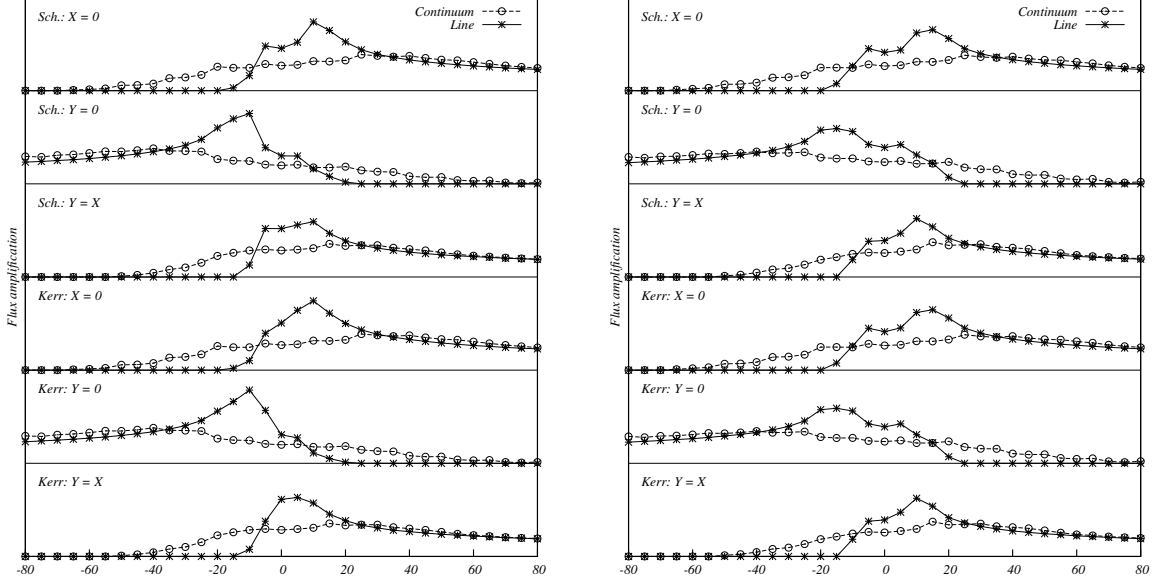


Fig. 6.— Variations of the Fe K $\alpha$  line and X-ray continuum flux during a caustic crossing (ERR=50  $R_g$ ) for the case (iv) of §2.2.1. We consider three different directions of caustic crossing ( $X=0$ ,  $Y=0$  and  $X=Y$ ; see §2.2.2). Left and right panels correspond to the black body and modified black body laws, respectively. From top to bottom, the three first panels (left and right) correspond to Schwarzschild and the last three to Kerr metrics. The flux axis ranges from 1 to 1.7.

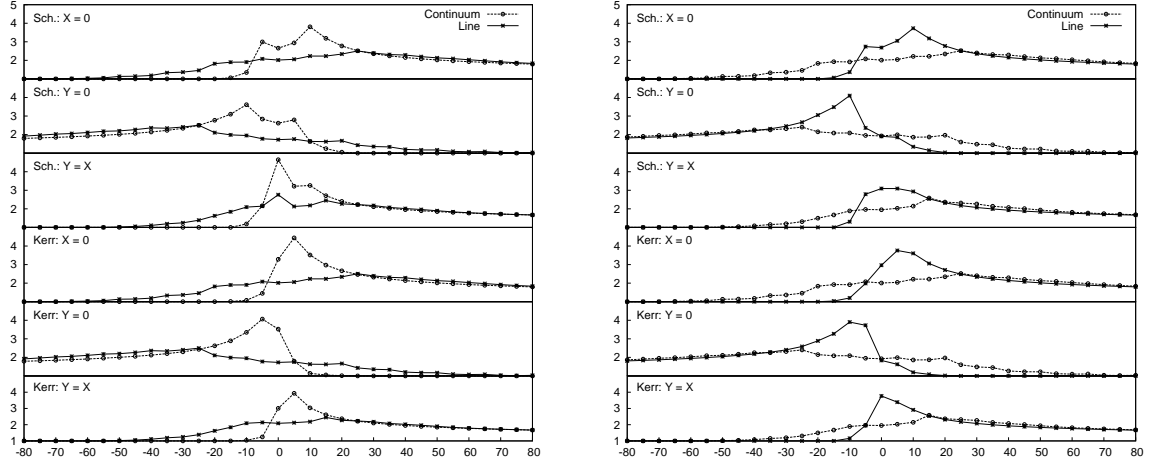


Fig. 7.— The same as in Fig. 5, but for the power-law radiation, the left panel corresponds to the case iii) and the right to the case iv) of §2.2.1

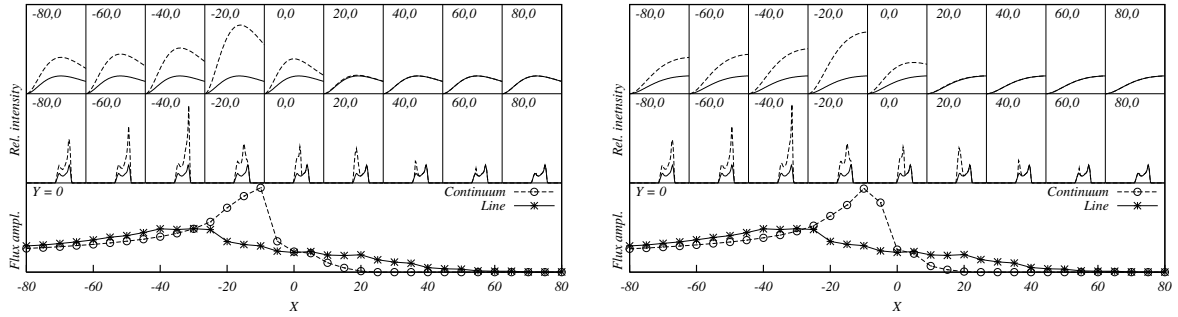


Fig. 8.— Variations of the X-ray continuum and the Fe K $\alpha$  line flux for a highly inclined disk ( $i = 75^\circ$ ) due to microlensing by a caustic with  $ERR=2000 R_g$ . Black body (left) and modified black body (right) are considered. The geometry corresponds to case (iii) of §2.2.1. The flux axis ranges from 1 to 4.

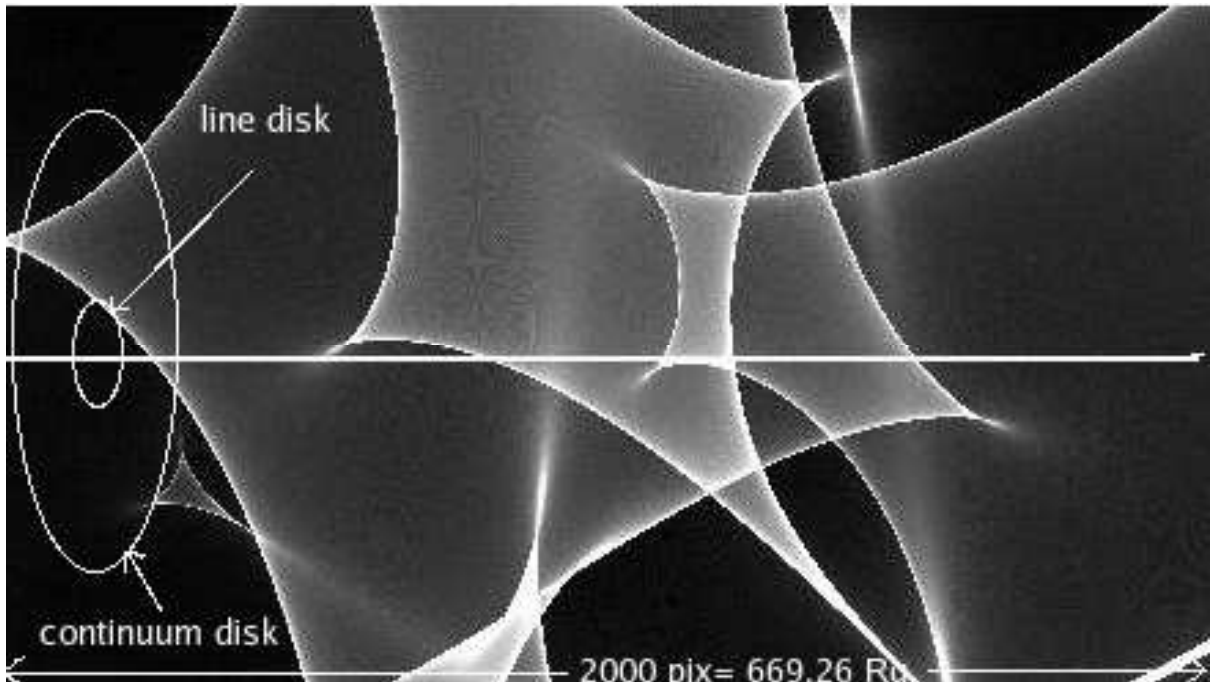


Fig. 9.— Microlensing map of QSO 2237+0305A image with  $1\text{ERR} \times 2\text{ERR}$  ( $1000 \text{ pix} \times 2000 \text{ pix} = 334.63 \text{ } R_g \times 669.26 \text{ } R_g$ ) on a side and scheme of the projected disk with outer radius  $R_{out} = 20 \text{ } R_g$  and  $100 \text{ } R_g$  for the Fe  $\text{K}\alpha$  line and the X-ray continuum, respectively. The straight line presents the path of the center of the disk (left side of the pattern corresponds to 0 pix).

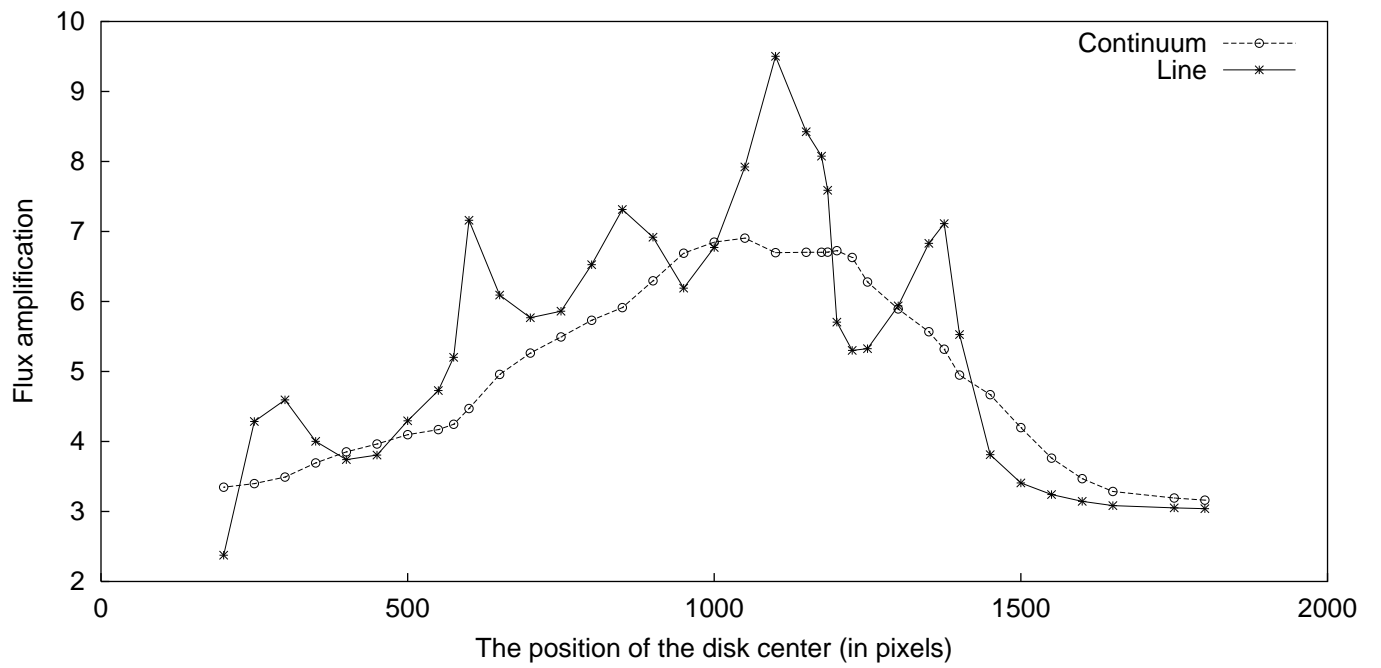


Fig. 10.— The amplification of the Fe K $\alpha$  line and the X-ray continuum total flux for different positions of the center on the microlensing map of QSO 2237+0305A image (see Fig. 9).

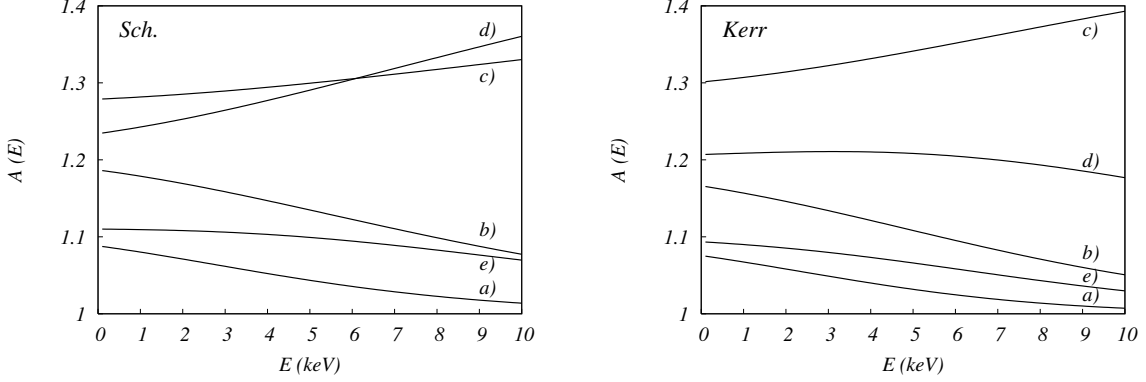


Fig. 11.— Microlensing amplification as a function of emitted energies (the chromatic effect of microlensing). The calculations were performed for caustic crossing along the rotation axis ( $Y=0$ ) for the following positions on X-axis: a)  $X=20 R_g$ ; b)  $X=10 R_g$ ; c)  $X=0 R_g$ ; d)  $X=-10 R_g$  and e)  $X=-20 R_g$ . We take  $ERR=50 R_g$ . The radii of the disk are  $R_{inn}=R_{ms}$ ,  $R_{out}=30 R_g$ . The black body emissivity law in both Schwarzschild (left) and Kerr metrics (right) is used in calculation.

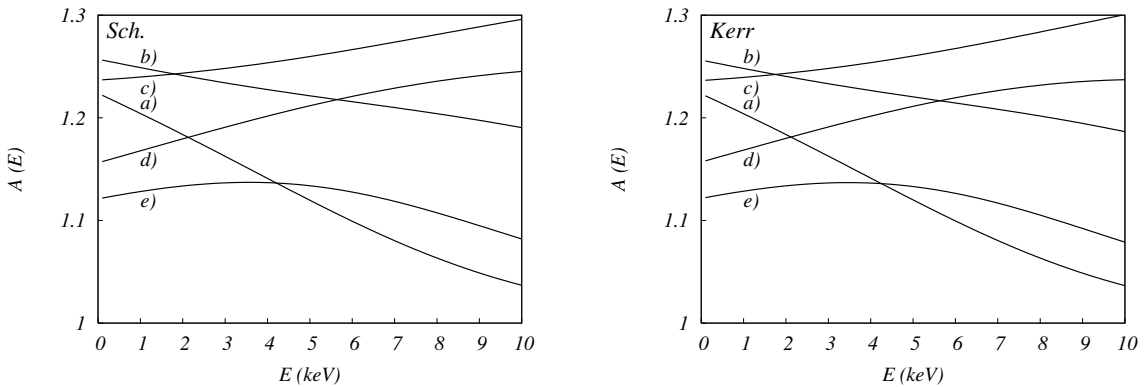


Fig. 12.— The same as in Fig. 11, but for the 'modified' black body law in Schwarzschild (left) and Kerr metric (right).

Table 1: Projected ERR (expressed in gravitational radii) for different deflector masses for the four lensed QSOs where microlensing of the Fe K $\alpha$  line is suspected: J0414+0534 - Chartas et al. (2002), QSO H1413+117 - Oshima et al. (2001a); Chartas et al. (2004), QSO 2237+0305 - Dai et al. (2003). Used values for the cosmological constants are:  $H_0 = 50 \text{ km s}^{-1}\text{Mpc}^{-1}$  and  $\Omega_0 = 1$ . The black hole mass is assumed to be  $10^8 M_\odot$ .

Object	$z_s$	$z_l$	$1 \times 10^{-4} M_\odot$	$1 \times 10^{-3} M_\odot$	$1 \times 10^{-2} M_\odot$	$1 \times 10^{-1} M_\odot$	$1 M_\odot$
MG J0414+0534	2.64	0.96	20.3	64.2	203.1	642.3	2031.1
QSO 2237+0305	1.69	0.04	11.2	35.4	112.1	354.5	1121.0
QSO H1413+117	2.56	1.00	19.8	62.5	197.7	625.2	1977.0